Bulletin of the Seismological Society of America. Vol. 59, No. 1, pp. 427–444. February, 1969

A Technique for the Analysis of Transient Seismic Signals

By A. Dziewonski*, S. Bloch and M. Landisman

Abstract

An analytical method, called the "multiple filter technique," is shown to be a fast and efficient means of studying multi-mode dispersed signals. Amplitudes and phases, as functions of period and velocity, are determined from the output of a set of narrow-band digital filters. The group velocities and other dispersion parameters determined by this technique are concordant with theoretical values when the method is tested with synthetic seismograms. It can recover broader portions of the dispersion present in ordinary seismic recordings compared to the classical peak and trough method. A simple diagnostic diagram is introduced in order to study the time and frequency resolution permitted by this analytic technique.

I. Introduction

The "multiple filter technique" is shown to be a fast, efficient method of analyzing multiply dispersed signals. The amplitudes and phases of signals passed by an array of narrow-band filters can be used to measure group velocity, relative excitation and transmission as functions of period and velocity, lateral refraction, modal vibrations of the surface, and other dispersion parameters associated with a variety of modes recorded by a single station for one event.

This technique can recover broader portions of the dispersion present in ordinary recordings, compared to the classical peak and trough method. This latter method often fails when the signal-to-noise ratio decays or when the signal is contaminated by other arrivals. Similar difficulties have been noted when the phase delay calculated by ordinary Fourier analysis has been differentiated in order to obtain the group velocity.

Digital methods have been used previously in dispersion studies, such as the investigation by Alexander (1963), who used frequency and velocity windows to isolate portions of the observed modes. Archambeau, Flinn and Lambert (1966) also used digital filters in a search for dispersion in body wave arrivals.

Recently, Landisman, Dziewonski and Satô (1969, which will be referred to as "Paper I" hereafter) developed an automated process called "moving window analysis", which produces a display of amplitudes and/or phases as functions of period and group velocity. These results were calculated by Fourier analysis of suitably windowed portions of the seismogram. Results produced by the multiple filter technique often show greater frequency resolution, when compared with those calculated by the moving window process. The present technique does not have the intrinsic period shift noted for the earlier method, and the results are obtained with a much smaller expenditure of computer time (Section II).

The dispersion parameters inferred from multiple filter analysis can be tested, using specially prepared synthetic seismograms. The measured results compare favorably with the theoretical values (Section III). A simple diagnostic diagram is introduced which may be used to study the results produced by the multiple filter technique for dispersion curves of various types. An analysis of the time and frequency resolution

* On leave from the Institute of Geophysics, Polish Academy of Sciences.

achieved for multi-mode propagation from a simulated "earthquake" and its "aftershock," with a small interval between their origin times, represents an illustrative example of the use of this type of diagram (Section IV).

The report represents another contribution to a continuing series of studies whose object is the extraction and interpretation of the wealth of information contained in ordinary seismograms (Bloch and Hales, 1968; Landisman, Dziewonski, Satô, and Massé, 1968; Paper I).

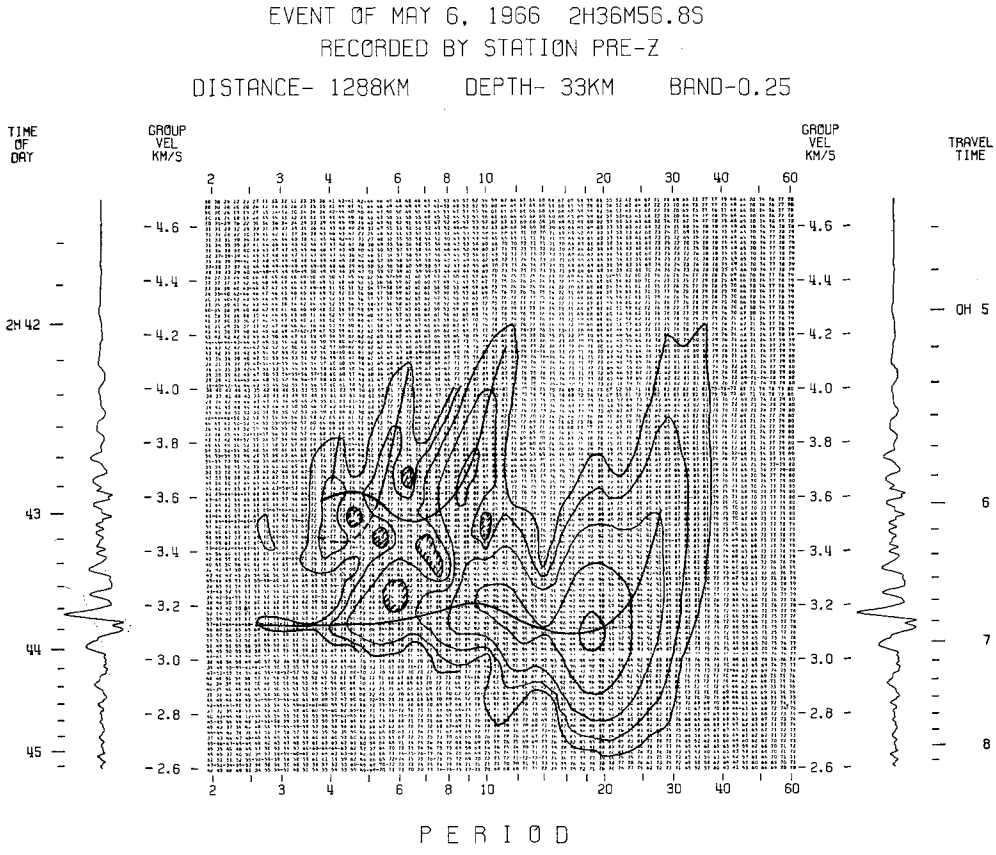

FIG. 1. Multiple filter analysis of surface waves. Magnitude 5.5 (USCGS) earthquake in southern Malawi, southeast Africa as recorded on long period vertical component of WWSSN observatory at Pretoria, S. Africa. Contours of relative energy (5 db interval) as a function of period and group velocity, corrected for instrumental system. Thick solid lines represent group velocities inferred from the contours (right to left): Rayleigh mode, first shear mode, second shear mode, third shear mode. Slower portion of second shear mode uncertain, marked with broken line.

II. MULTIPLE FILTER TECHNIQUE

The multiple filter technique can resolve complex transient signals composed of several dominant periods that arrive at the recording station almost simultaneously. Instantaneous spectral amplitude, presented in db as a function of period and group velocity, may be interpreted in terms of multi-mode group velocity. These amplitudes and the corresponding phases are displayed in a manner which is similar to that employed for moving window analysis (Paper I). When mutually orthogonal components of the motion are analyzed, the results can be used to study the three-dimensional

vibration of the recording site in terms of the ellipticity and phase for each of the observed propagating modes. Quantitative determinations of lateral refraction and separation of wave types are also possible.

A. An example of analysis using the multiple filter technique. Figure 1 presents an analysis of the long-period vertical recording from the World Wide Standard Seismograph Network (WWSSN) Observatory at Pretoria, S. Africa, for an earthquake which occurred in southern Malawi on 6 May 1966 at 02:36:56.8 GMT. Instantaneous spectral amplitude in db, as a function of group velocity and period, has been contoured after normalization to a maximum value of 99 db. Contours are usually drawn

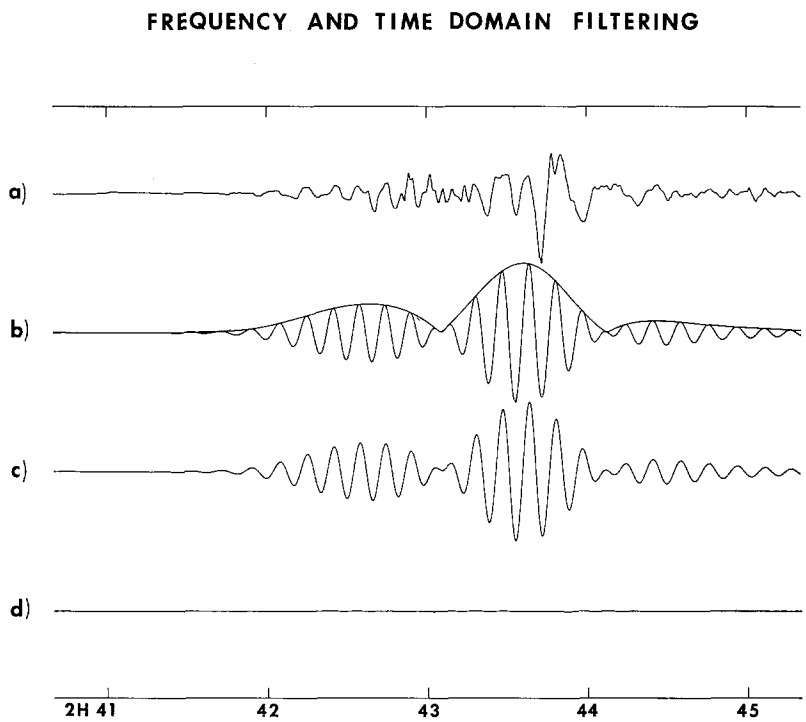

FIG. 2. Comparison of results of filtering in frequency and time domains. (a) Seismogram of Figure 1. (b) Trace (a) filtered in frequency domain for period 10 sec. Envelope calculated from in-phase and quadrature filtered traces. For details see text, section II B. (c) Trace (a) filtered in time domain. (d) Difference between traces (b) and (c).

at 1 db intervals for interpretation of the analysis, but here they are shown only at 5 db intervals for clarity of presentation. Amplitude minima are indicated by hatched areas. The analyzed recording is presented with a linear velocity scale at both sides of the display for comparison with the contours. The dispersion inferred for each of the modes is indicated by the lines along the ridge crests of the contour diagram.

The Rayleigh mode and the first three shear modes have been identified in Figure 1. The dispersion observed for the Rayleigh mode is typically continental: the group velocity has a minimum at a period of about 19 sec, a maximum near 10 sec (Rg) and a short period branch extends to 2.5 sec with nearly constant velocity, confirming the high surface velocities present in this area.

The ridge crest which runs from 12 to 3.5 sec is interpreted as the first shear mode. The steeply descending portions of the second and third shear modes are also indicated. The short period extension of the second shear mode is delineated with a broken line,

since the trend of its dispersion curve is uncertain for velocities lower than those of the first shear mode.

The amplitude display in Figure 1 represents only a part of the information available in the seismogram. The uses of the phase information will be demonstrated in another section.

B. Filtering and Evaluation of Instantaneous Spectral Amplitude and Phase. Each of the columns in Figure 1 consists of sampled values of instantaneous spectral amplitude (in db) which are calculated from the original seismogram by filtration with a band-pass filter centered about the corresponding period. This filtration could have been performed either in the time domain or in the frequency domain, since both of these processes are theoretically equivalent. Somewhat different results are often obtained in practice, however, because the record length and the sampling rate are both finite. Truncation of the time domain filter weights may also contribute to observed discrepancies.

Figure 2 shows a comparison of filtration in the time and frequency domains. Trace (a) is the unfiltered record whose analysis was shown in Figure 1. Trace (b), which appears immediately below, represents the result of filtration in the frequency domain for the period 10 seconds. The equivalent filter operating in the time domain produced trace (c) and the difference between these two signals is shown as trace (d). Traces (b), (c), and (d) have been normalized independently of trace (a). The local maxima of the amplitude envelope visible on traces (b) and (c) correspond to the first shear mode and the Rayleigh mode, respectively. The difference signal (d) is small: the largest deviations, which never exceed 1 per cent of the maximum amplitude of the filtered traces, occur at the points of transition between the modes.

Even though both processes have produced results which may be considered identical for all practical purposes, filtration in the frequency domain has definite advantages over its time domain equivalent. First, it is possible to use filter functions whose inverse transforms cannot be expressed in terms of elementary functions. Also, operations in the frequency domain may be accomplished with a considerable saving of computer time, since the execution of the fast Fourier algorithm (Cooley and Tukey, 1965) is usually several times faster than the corresponding convolution in the time domain, for the same precision.

The multiple filter technique is used to study variations of amplitude (or energy) of a signal as a function of velocity (time) and period (frequency). It is desirable, therefore, that the filtering function should have good resolution in the immediate vicinity of each center frequency and velocity value. The Gaussian function was chosen to meet these requirements.

A system of filters with constant Q is appropriate for the analysis of most dispersed seismic signals, since this leads to constant resolution on a log-period scale. If ω_n denotes the center frequency for the nth column, the window function can be written

$$H_n(\omega) = e^{-\alpha \cdot \left(\frac{\omega-\omega_n}{\omega_n}\right)^2}. \tag{2.1}$$

The Fourier transform of $H_n(\omega)$ is

$$h_n(t) = \frac{\sqrt{\pi} \cdot \omega_n}{2\alpha} \cdot e^{-\frac{\omega_n^2 \cdot t^2}{4\alpha}} \cdot \cos(\omega_n t). \tag{2.2}$$

The resolution is controlled by the parameter α. Improved resolution in one domain

causes the inverse effect in the other, but the value of the product of the RMS durations of the Gaussian function, $D_\omega \cdot D_t$, remains constant (for definitions see Papoulis, 1962, section 4-4). The value chosen for the parameter α depends upon the nature of the dispersion in the seismogram.

Another important property of the Gaussian function is that of all the possible non-band-limited functions, the product of its RMS durations is a minimum (for proof see ibid.). This means that the frequency-time resolution, which can be measured as $1/D_\omega \cdot D_t$, is greater for the Gaussian function than that for any other type of non-band-limited function. In practical computations, however, it is usually convenient to truncate the low amplitude ends of the function (2.1) in order to avoid unnecessary calculations, even though it becomes a band-limited function. Dr. F. Abramovici (personal communication) pointed out to the authors that Slepian, Pollack and Landau (1961) have shown that the highest possible energy concentration of the impulse response corresponding to a band limited filter function is achieved when the filter is a truncated prolate spheroidal wave function of zero order (see also Papoulis, 1962, section 4-5). If, however, the Gaussian function is truncated at a value of the order of 30 db down from the maximum, the energy concentration of its impulse response is only 0.1 per cent lower than that of the corresponding prolate spheroidal wave function. The cut-off level applied in this paper is at least 30 db down from the maximum; therefore, the Gaussian function, which is simpler to evaluate, can for all practical purposes be considered as equivalent to the optimum filter function.

Let the relative bandwidth be designated BAND, then the lower and upper band limits of the symmetrical filter, denoted as $\omega_{l,n}$ and $\omega_{u,n}$, respectively, are

$$\omega_{l,n} = (1 - \text{BAND}) \cdot \omega_n \tag{2.3a}$$

$$\omega_{u,n} = (1 + \text{BAND}) \cdot \omega_n . \tag{2.3b}$$

The parameter β, which describes the decay of the window function, is determined by the desired value of the function at the band limits

$$\beta = \ln \left[\frac{H_n(\omega_n)}{H_n(\omega_{l,n})} \right] = \ln \left[\frac{H_n(\omega_n)}{H_n(\omega_{u,n})} \right]. \tag{2.4}$$

Parameter α of equations (2.1) and (2.2) can be expressed in the terms of BAND and β,

$$\alpha = \beta / \text{BAND}^2 \tag{2.5}$$

and the window function is

$$H_n(\omega) = \begin{cases} 0 & ; \text{ for } \omega < (1 - \text{BAND}) \cdot \omega_n \\ e^{-\alpha \left(\frac{\omega - \omega_n}{\omega_n} \right)^2} & ; \text{ for } (1 - \text{BAND}) \cdot \omega_n \leqq \omega \leqq (1 + \text{BAND}) \cdot \omega_n \\ 0 & ; \text{ for } \omega > (1 + \text{BAND}) \cdot \omega_n . \end{cases} \tag{2.6}$$

Trace (b) of Figure 2 is the filtered seismogram, after windowing in the frequency domain with the truncated Gaussian function (2.6). The parameters are $\omega_n = 0.628$, BAND = 0.25, $\beta = 3.15$ ($\alpha = 50.3$). Trace (c) represents the convolution of trace

(a) with a weighting function derived from equation (2.2), and calculated with 1001 points symmetrically distributed over a 200 sec interval centered at t_0.

Application of a system of filters with a constant relative bandwidth represents an additional asset in the log-period scale of Figure 1, since the total width of each of the filters corresponds to the same number of columns, for each of the center frequencies. In certain cases it may be useful to apply systems of filters for which the relative bandwidth varies as a function of frequency. An example of analysis with a *constant* bandwidth will be discussed later (Figure 9).

The inverse Fourier transform of the seismic spectrum as windowed by the function (2.6) gives only the in-phase filtered signal for each ω_n. Knowledge of the quadrature time function is also required for evaluation of the instantaneous spectral amplitudes $A_n(t)$ and phases $\varphi_n(t)$ as defined by Goodman (1960)

$$A_n(t) \cdot e^{i\varphi_n(t)} = h_n(t) + iq_n(t). \tag{2.7}$$

The in-phase and quadrature time functions are designated by $h_n(t)$ and $q_n(t)$.

The quadrature spectrum $Q_n(\omega)$ is easily found from the in-phase spectrum,

$$Q_n(\omega) = H_n(\omega) \cdot e^{i\pi/2}. \tag{2.8}$$

In terms of the Fourier series, where a_k and b_k denote the cosine and sine coefficients of the in-phase spectrum, and a_k' and b_k' are the corresponding coefficients of the quadrature spectrum,

$$a_k' = -b_k, \qquad b_k' = a_k. \tag{2.9}$$

After inverse transformation, the instantaneous amplitudes and phases are

$$A_n(t) = [h_n^2(t) + q_n^2(t)]^{1/2} \tag{2.10a}$$

$$\varphi_n(t) = \tan^{-1}[q_n(t)/h_n(t)]. \tag{2.10b}$$

A graphical example of an envelope $A_n(t)$ is shown in Figure 2, where it is displayed along the crests of trace (b). The values of the amplitudes in Figure 1 in the column corresponding to a period of 10 sec are the db equivalent values of this envelope at equal intervals of velocity. Note that the maxima of the envelope do not coincide with any of the peaks or troughs of the filtered signal.

An equivalent result could have been obtained by filtering the seismogram in the time domain with a quadrature filter, as suggested by Ormsby (1961).

C. Description of the flow-chart. A description of the multiple filter process is shown in the flow-chart in Figure 3.

(1) A seismogram digitized at a constant rate is entered into the computer and its mean and linear trend are removed. The digitization rate must be sufficient to prevent aliasing by the highest frequencies present in the seismogram. The rate ranged from 1 to 5 samples per second for the cases presented in this study.

(2) The observed time series is expanded to a suitable power of 2 by adding an appropriate number of zeros. The length of the expanded series is primarily determined by the requisite frequency resolution. A length of 8192 (2^{13}) samples has been used throughout this study. The time function is then converted into a sine and a cosine series using the Cooley-Tukey (1965) algorithm for fast Fourier transformation.

(3) Instrumental distortions of phase and amplitude may be removed in the com-

plex domain at this stage, by correcting for the real and imaginary parts of the instrumental response.

(4) The array of center frequencies, which are related by a constant ratio, is evaluated for the filters which will be used next. The length of the time series and the sampling rate determine the frequency of the harmonic components obtained from the Fourier series. It is usually impossible to find the exact counterparts of the elements of the array among these harmonics. Those harmonics which are closest to each member of the array are selected and substituted as center frequencies for further processing. In the cases presented in this paper, the maximum deviation of the harmonics from the array frequencies was always less than 1.5 per cent ($\frac{1}{4}$ of the change of frequency between adjacent columns) and in general was much less. The periods which are used to label columns in Figure 1 correspond to the array of frequencies related by the constant ratio discussed above.

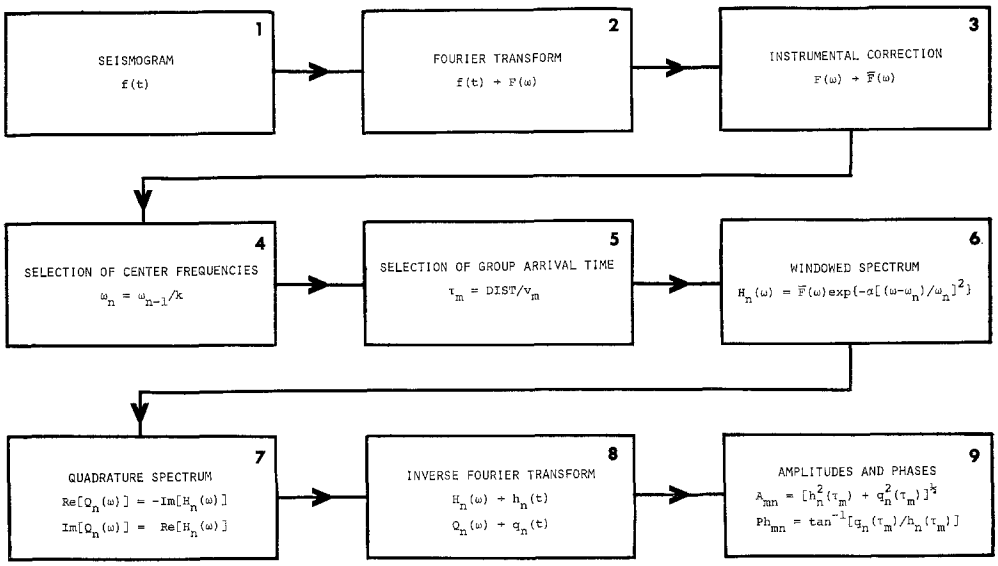

FIG. 3. Flow-chart of the multiple filtering analysis process.

(5) An array of times is found for the preselected values of group velocity (rows of the Figure 1).

(6) Filtration is accomplished by windowing the seismic spectrum with a filter function which is symmetric about the current center frequency.

(7) The quadrature spectrum is formed for calculation of the instantaneous spectral amplitudes and phases.

(8) The inverse Fourier transforms of the in-phase and quadrature spectra are computed with the same algorithm for fast Fourier transformation, which was used in step 2.

(9) Instantaneous spectral amplitudes and phases are computed for each of the group arrival times.

The procedure described in points 6 through 9 must be repeated for each center frequency.

III. TEST OF THE MULTIPLE FILTER TECHNIQUE

A. Synthetic Seismograms. Some simple synthetic seismograms were constructed in order to test the precision and resolving power of the multiple filter technique. These

seismograms are by no means intended to represent the real Earth. The only purpose of their construction was their use in these tests.

Theoretical phase velocity dispersion curves for the fundamental Love, Rayleigh and first shear modes were used in the construction of the synthetic seismograms. The medium response, attenuation and instrumental response were not taken into consideration. A symmetric time function was chosen for the source, and the phases for

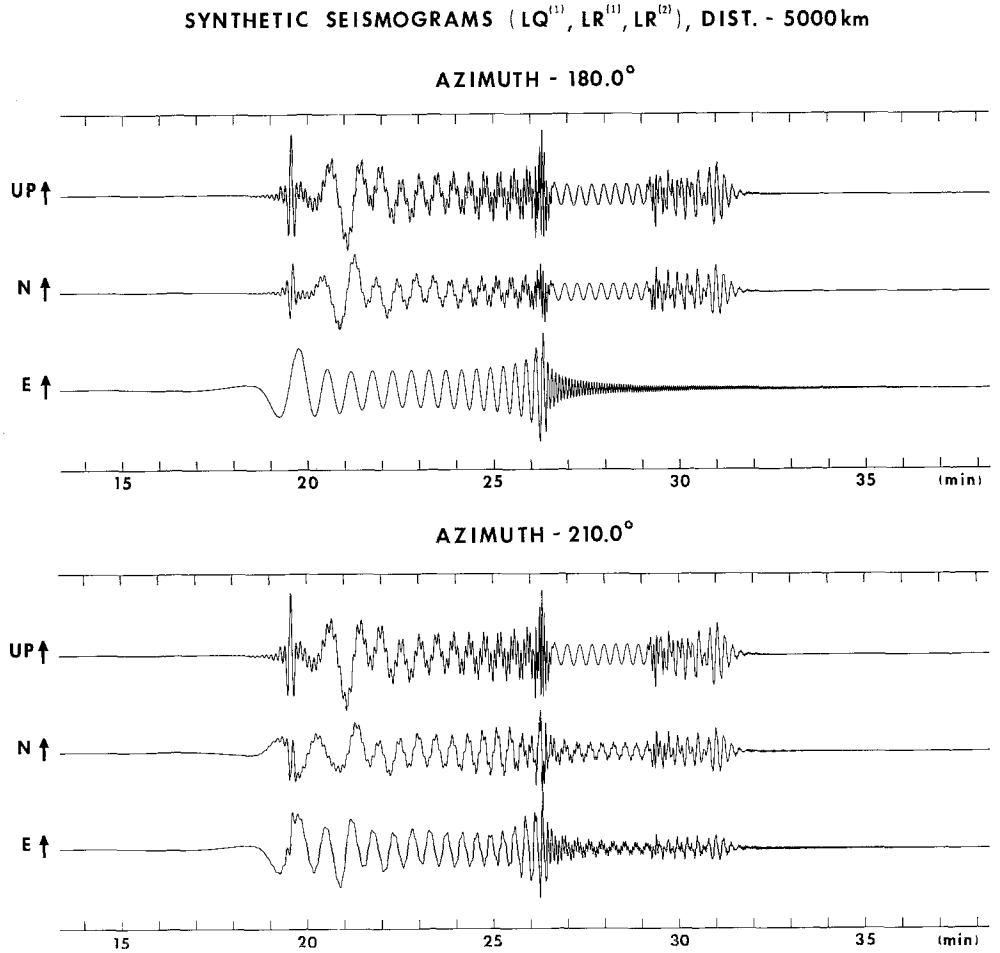

FIG. 4. Test signals: three-component synthetic seismograms, containing Rayleigh mode, first shear mode and fundamental Love mode from azimuths of 180° and 210° for an epicentral distance of 5000 km.

each of 2^{12} (4096) harmonics were computed for a given path length for each of the three modes above. The amplitude spectrum was arbitrarily chosen so that the synthesized time functions would roughly resemble observed seismograms.

The combined spectrum was obtained by a summation of the complex harmonic components for each mode. The ellipticity for the Rayleigh mode was assumed to have the constant value of $-0.8i$, assuring retrograde elliptical motion. The ellipticity for the first shear mode was taken to be $+0.5i$, which corresponds to prograde motion.

The cited algorithm was used to transform the harmonic components into a time series.

Two sets of three-component synthetic seismograms are shown in Figure 4. It was assumed that the source was south of the point of observation for the first set, and an azimuth of 210° was assumed in the second case.

Figure 5 shows the result of processing the vertical synthetic seismogram by the multiple filter technique for periods from 3 to 120 sec. The synthetic seismogram was computed for a distance of 5000 km, with a sampling rate of 4 samples/second.

The amplitude contours are drawn at 5 db intervals (thin lines). Local amplitude

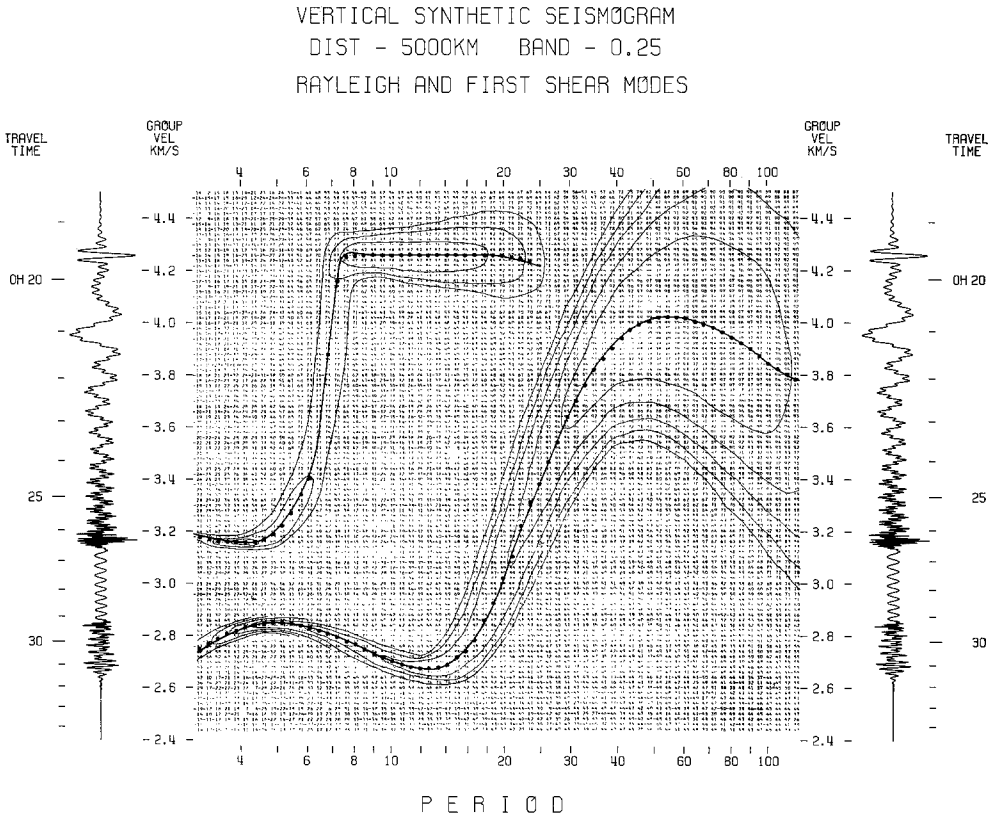

FIG. 5. Multiple filter analysis of vertical component synthetic seismogram of Figure 4. Contours of relative energy at 5 db intervals. Thick lines show theoretical group velocities of the Rayleigh mode and the first shear mode. The dots represent values of group velocity inferred from the contour diagram.

maxima along each of the columns are flagged with a minus sign to assist in the interpretation of the contour diagram. These marks are particularly useful at the slowly changing portions of the group velocity curves (Airy phases). The amplitudes can be presented on a linear scale for improved resolution of values within 20 db of the maximum. However, in seismograms where the signal has a large dynamic range, the logarithmic amplitude scale is preferable.

In Figure 5, the theoretical group velocities for the Rayleigh and first shear modes are drawn with thick lines. The black dots represent group velocities inferred from the contours. The difference between the interpreted and theoretical curves does not exceed 0.01 km/sec.

In this theoretical case a precise interpretation of group velocities was possible for amplitudes as small as 40 db below the maximum amplitude. The "noise" in this case

is associated with the finite length of record, the discrete sampling rate and the computer word length.

The prominent features of the synthetic seismogram can be related to the configuration of the group velocity dispersion curves, although their relative amplitudes are arbitrary since no attempt was made to model the medium response. The large amplitude at 4.26 km/sec corresponds to the extended flat portion of the first shear mode between the periods from 7 to 25 sec. The Rayleigh mode Airy phase maximum occurs

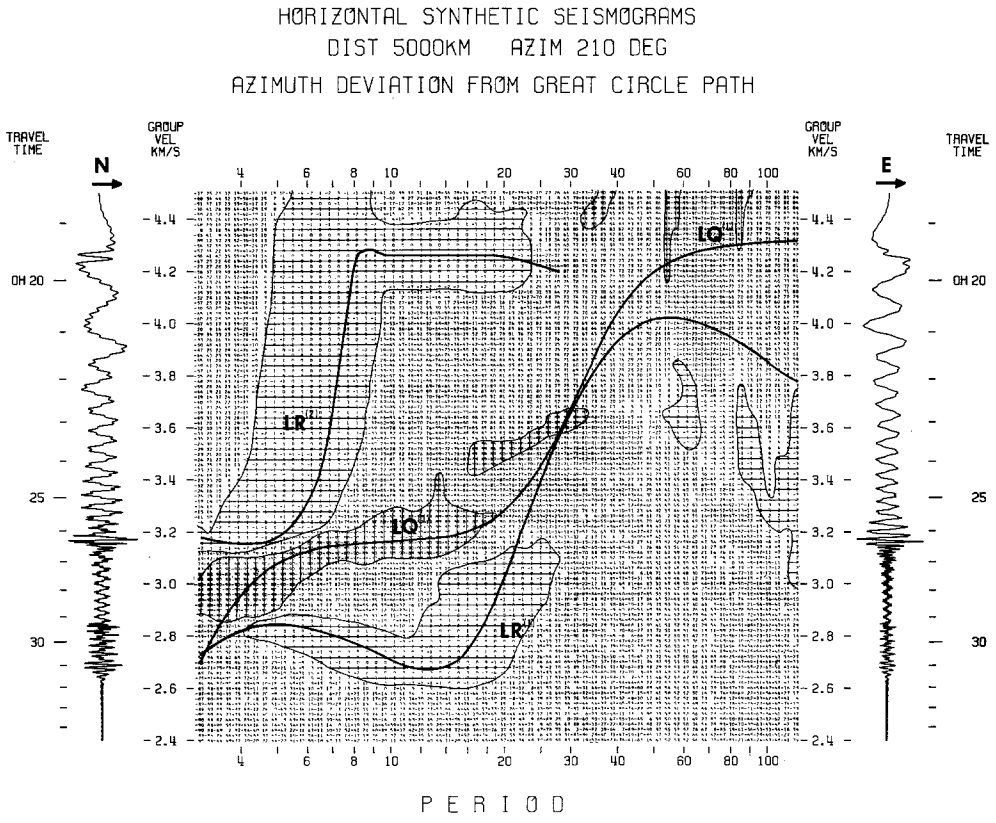

FIG. 6. Azimuthal deviations of the longer axis of the instantaneous horizontal particle motion ellipse from the propagation path along the "station-epicenter" great circle, as calculated from amplitudes and phases obtained by multiple filter analysis of the horizontal synthetic seismograms in Figure 4 for a source at an azimuth of 210°. Thick solid lines show theoretical group velocities for modes identified in the figure. Areas marked with horizontal stripes correspond to deviations within ±3° of the path of propagation, areas covered with vertical stripes correspond to deviations from 87° to 93°.

at a velocity of 4.02 km/sec for periods near 55 sec. The next prominent feature, represented by the large amplitudes of high frequency at 3.16 km/sec, corresponds to the Airy phase of the first shear mode at 4.3 sec. The rather complex portion of the seismogram between 2.85 km/sec and 2.60 km/sec is associated with the Rayleigh mode dispersion for periods from 3 to 18 sec. The curve has two Airy phases within this interval, a minimum near 13.5 sec and maximum near 5 sec.

The comparison in Figure 5 serves only as a test of the instantaneous spectral amplitudes. The instantaneous spectral phase values play an important role in the analysis of three-component recordings. Evaluation of the parameters of the horizontal motion ellipse can be used to test the precision of the phases obtained by the multiple filter technique.

The motion in the horizontal plane can be described by an ellipse which is appropriate for each of the frequencies and velocities analyzed. The azimuths and amplitudes of the axes of this set of ellipses represent a useful tool for mode identification, as well as the measure of mode interference and noise contamination. A method for evaluating the parameters of these ellipses, based on the instantaneous horizontal amplitudes and phases, is described in Paper I, section 4. Figure 6 shows a display of azimuthal differences between the longer axis of the horizontal motion ellipse and the great

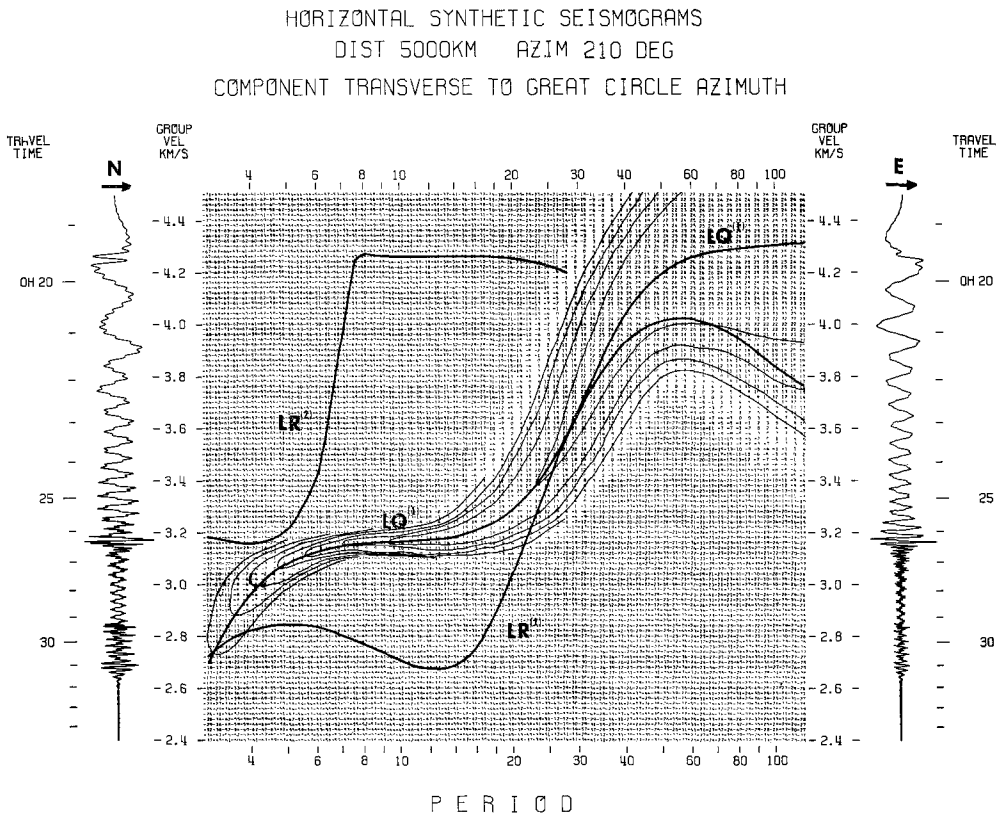

FIG. 7. Contour diagram of the component transverse to the "station-epicenter" great circle path computed from amplitudes and phases determined by multiple filter analysis of the horizontal synthetic seismograms of Figure 4 for a source at an azimuth of 210°. Contour interval—5 db. Thick solid lines show theoretical group velocities for modes identified in the figure. Note concordance of contours to the theoretical group velocity curve for the Love mode, even in regions marked by strong interference with the Rayleigh mode on the N and E seismograms, left and right.

circle path as a function of frequency and velocity. The areas on the figure marked with horizontal lines correspond to azimuthal differences of 3° or less. Areas marked with vertical lines correspond to deviations between 87° and 93°. The theoretical group velocities for the Love, Rayleigh and first shear modes are marked with thick lines. The measured deviations are appropriate to the type of propagation for periods shorter than 20 sec. At longer periods there is strong interference between the Rayleigh and Love modes.

The transformation of coordinates in the horizontal plane represents another type of analysis for which the phase information is required. Rotation of coordinates is performed on the elements of the matrices themselves, not on the time domain representation of the seismograms (ibid, equations 4.1 and 4.3). Figure 7 shows the contour

diagram for the component transverse to the great circle path. The values used here were the amplitudes and phases calculated for the N-S and E-W components of the synthetic seismograms from a source at an azimuth of 210° from the observation site. If these values were correct, the computed grid of amplitudes would contain only the fundamental Love mode.

The amplitudes in Figure 7 are presented in an unnormalized db scale. The contours clearly delineate the Love mode, and the inferred dispersion compares favorably

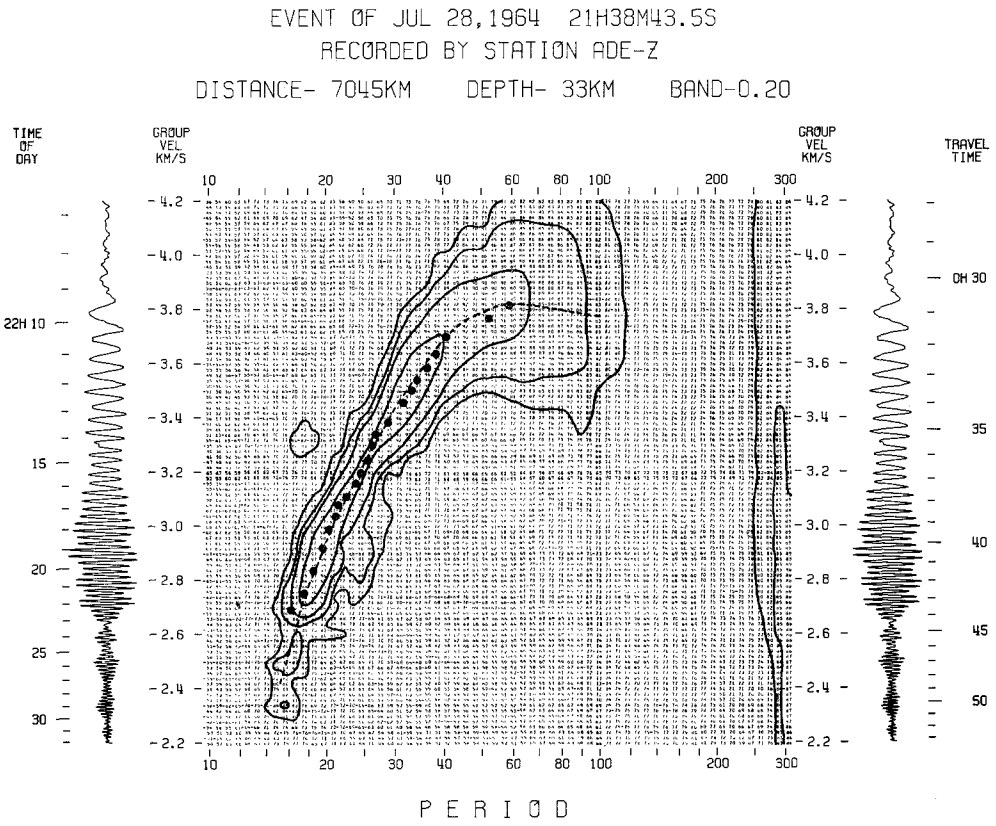

FIG. 8. Multiple filter analysis of Rayleigh waves from magnitude 5.5 (USCGS) earthquake, Andaman Sea west of northern Malay peninsula, recorded on long period vertical component of WWSSN observatory at Adelaide, southern Australia. The broken line is the apparent group velocity interpreted from the contours; black dots represent group velocities determined from the measurement of peaks and troughs *vs* arrival time.

with the analysis of a synthetic Love wave seismogram as well as with the theoretical group velocity for this mode. The overall signal-to-noise ratio is approximately 60 db and this ratio does not change in the neighborhood of the dispersion curves for the Rayleigh and first shear modes.

B. Observed Seismograms. Although satisfactory results are indicated for the multiple filter analysis of synthetic seismograms, these seismograms represent highly idealized conditions which usually will not be duplicated for ordinary teleseismic recordings.

Group velocities interpreted from the contour diagrams were compared with peak and trough determinations as an additional test of the multiple filter technique. Two examples of these comparisons are presented in Figures 8 and 9.

Figure 8 shows the analysis of the long period vertical recording of an earthquake which occurred beneath the Andaman Sea at 21:38:43.5 GMT on 28 July 1964, 7045 km from the WWSSN station at Adelaide, Australia. About 70 per cent of the path was continental. The Rayleigh wave train has few beats, an indication that there is little contamination by non-least-time arrivals. The black dots represent the result of group velocity measurements by the peak and trough method. At the shorter periods they lie within 0.02 to 0.03 km/sec from the dashed line which represents the interpretation of the contours. The multiple filter technique also shows the long-period extension of the group-velocity curve, while measurements by the peak and trough method are extremely difficult if not impossible in this period range.

Filters with constant relative bandwidth were applied in all the previous examples. Filters with a constant bandwidth can be used when more frequency resolution is required at the shorter periods. An example of this type of analysis is shown in Figure 9. The seismogram was recorded at Charters Towers, Australia, 8513 km from a Rat Island earthquake which occurred at 21:44:17.2 GMT on 29 April 1963. The record is highly contaminated with non-least-time arrivals, some of which were generated by lateral refractions at the beginning and/or the end of the long oceanic path.

Constant bandwidth filters were used in this case to resolve the non-least-time arrivals at shorter periods, since greater frequency resolution is needed to discriminate between the primary and numerous secondary arrivals in the steeply descending portion of the group-velocity curve.

The dots show the results of peak and trough analysis, in which the arrival time versus peak-number curve was heavily smoothed and more weight was given to the first arrivals. The non-least-time arrivals can be clearly seen on the contour diagram. Their amplitudes sometimes exceed those of the signal arriving at the same time. For example, at a velocity of about 2.8 km/sec the delayed arrival at 20 sec has an amplitude which is 4 db greater than that of the signal at 17 sec period. This frequency discrimination could be achieved only with the extremely narrow band filters used in this case. The dashed line generally lies within 0.02 km/sec of the peak and trough determination, except for the short-period end where the signal-to-noise ratio is poor. The range of the group velocity curve, as determined by the multiple filter technique, can be extended to periods as great as 300 sec with other filter parameters.

IV. Diagnostic Diagrams

The pattern of amplitudes produced by multiple filter analysis is also a function of the filter parameters. The invariance of the time $-$ bandwidth product determines the time resolution for each value of frequency resolution. This relationship is expressed by equations (2.1) and (2.2) for the Gaussian filter of constant relative bandwidth, which was used in all but one of the previous examples.

A diagnostic process has been designed to examine possible distortions in the amplitude display caused by the interference between different branches of complex seismic signals. It can also be used to study the ability of this technique to resolve a slightly delayed aftershock from the main event.

Consider a simple form of single mode dispersion, when the group velocity $u(T)$ is a monotonic function of the period T. The amplitudes $\mathcal{A}$ along the ridge crest of the corresponding contour diagram are $\mathcal{A}(u(T), T)$. If this ideal case were analyzed with filters of infinitely high resolution for both frequency and time, the values in the grid would be zero, except along the ridge crest. In practice, any element of the grid will be non-zero, since the time and frequency resolution are finite and surrounding elements

will contribute to the calculated amplitude value. Each element of the grid of amplitudes, $A_{nm}(v_n, T_m)$, is influenced by: (1) the amplitude on the ridge crest at the group velocity v_n, $\mathfrak{A}(u(T_j) = v_n, T_j)$, because of the finite frequency resolution and (2) the amplitude on the ridge crest at the period T_m, $\mathfrak{A}(u(T_m), T_m)$ because of the finite time resolution. If the values $\mathfrak{A}(u(T), T)$ and the filter parameters are known, it is

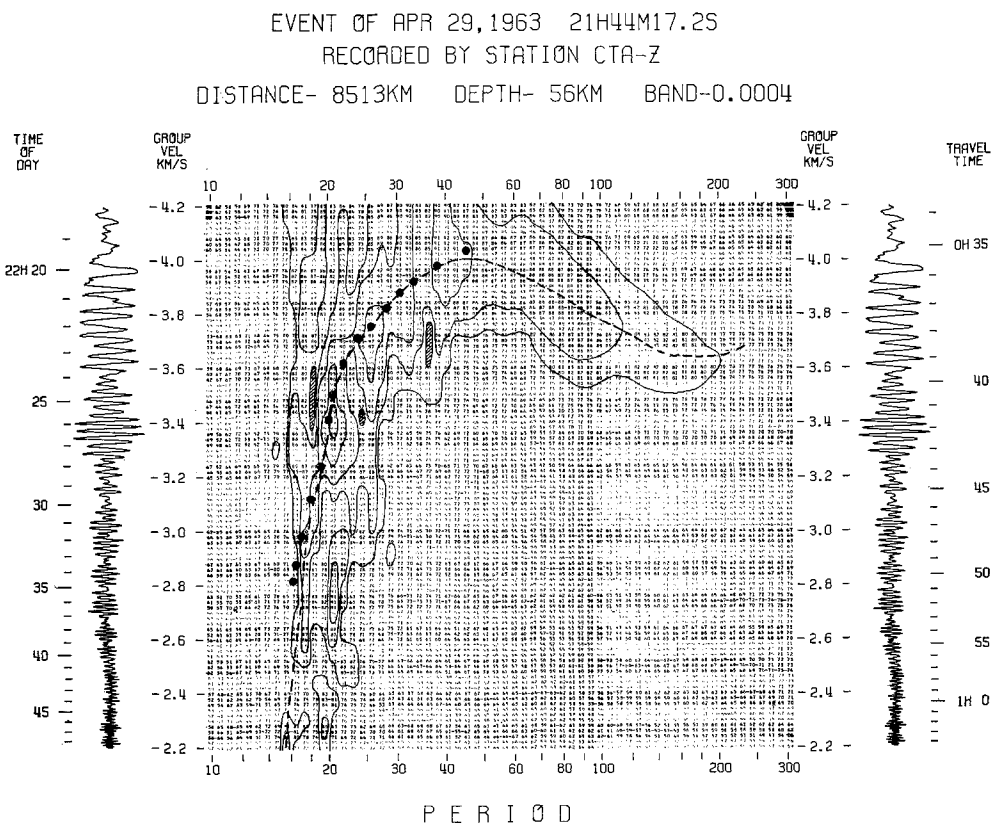

FIG. 9. Multiple filter analysis of oceanic Rayleigh waves. Magnitude 5.9 (USCGS) earthquake near Rat Island (Aleutian Arc) recorded on long period vertical component of WWSSN observatory at Charters Towers, northeastern Australia. The analysis has been performed with filters having *constant* bandwidth; in all previous examples the *relative* bandwidth was constant. Broken line shows apparent group velocity inferred from the contours, black dots represent group velocities determined from the measurement of peaks and troughs *vs* arrival time. Note that non-least-time dispersed arrivals may have higher energy than dispersed first arrivals.

possible to estimate the influence of the finite time and frequency resolution at all points on the grid.

The problem becomes more complicated when several branches of the same mode, higher modes or an additional event are also present. At each element of the grid it is possible to measure the interference between two or more multi-branched dispersion curves. Equation (2.1) shows that the relative influence of one mode on another mode because of the finite resolution in the frequency domain can be expressed as

$$B_{nm}^{(1)} = \frac{\mathfrak{A}^{(1)}(v_n, T^{(1)}(v_n))}{\mathfrak{A}^{(2)}(v_n, T^{(2)}(v_n))} \cdot \exp\left[-\alpha\left(\frac{T_m - T^{(1)}}{T^{(1)}}\right)^2\right]. \tag{4.1a}$$

The effects caused by the finite temporal resolution in expression (2.2) can be written

$$C_{nm}^{(1)} = \frac{\mathfrak{A}^{(1)}(u^{(1)}(T_m), T_m)}{\mathfrak{A}^{(2)}(u^{(2)}(T_m), T_m)} \cdot \exp\left[-\frac{\pi^2}{\alpha T_m^2} \cdot \left(\frac{\mathrm{DIST}}{u^{(1)}(T_m) - v_n}\right)^2\right]. \tag{4.1b}$$

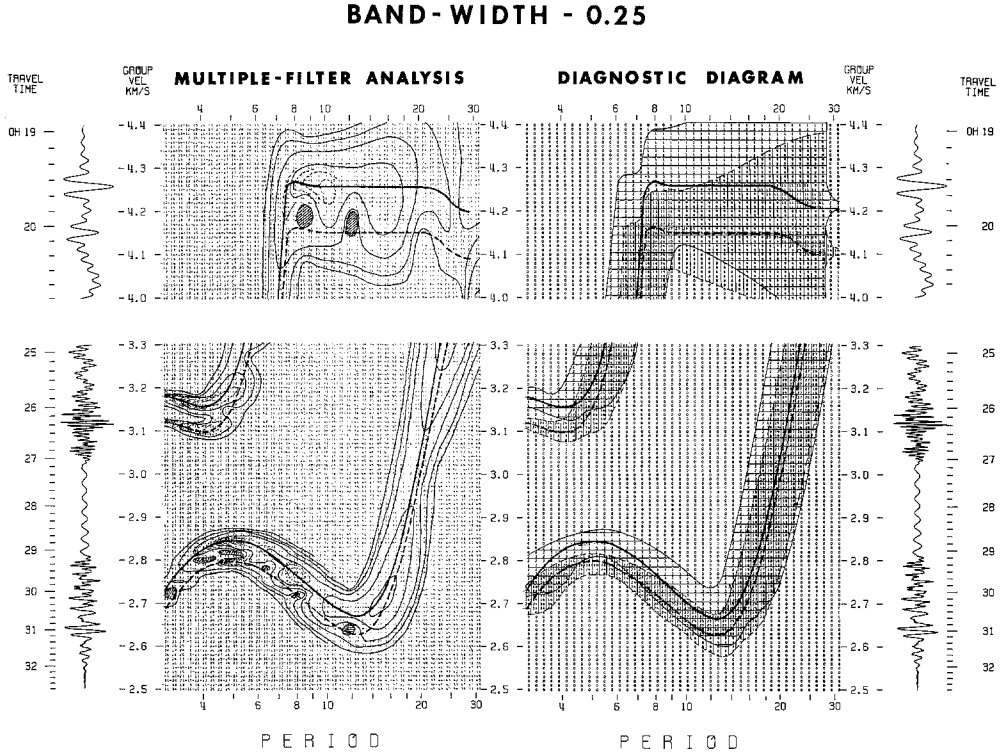

FIG. 10. Multiple filter analysis (left) and a corresponding diagnostic diagram (right) of two fragments of a synthetic seismogram with an "aftershock." The vertical component synthetic seismogram of Figure 4 has been diminished in amplitude by a factor of 0.5, delayed by 30 sec and then added to an original version of itself. Relative bandwidth for multiple analysis = 0.25. Thick solid lines represent theoretical group velocities for original signal, dashed lines show group velocities for the delayed signal. The interval of solid line contours on the left side of the figure is 5 db, broken contours, drawn in regions of particular interest, show 1 db amplitude variations. Hatched areas are amplitude lows. Areas under influence (with 20 db cut-off level) of the original signal are marked in the diagnostic diagram with horizontal stripes, areas under influence of the delayed signal are marked with vertical stripes. For explanation of numbers in the grid of diagnostic diagram see text, section 4.

Corresponding equations for the influence of the second mode on the first one are

$$B_{nm}^{(2)} = \frac{\mathfrak{A}^{(2)}(v_n, T^{(2)}(v_n))}{\mathfrak{A}^{(1)}(v_n, T^{(1)}(v_n))} \cdot \exp\left[-\alpha\left(\frac{T_m - T^{(2)}}{T^{(2)}}\right)^2\right] \tag{4.1c}$$

$$C_{nm}^{(2)} = \frac{\mathfrak{A}^{(2)}(u^{(2)}(T_m), T_m)}{\mathfrak{A}^{(1)}(u^{(1)}(T_m), T_m)} \cdot \exp\left[-\frac{\pi^2}{\alpha T_m^2} \cdot \left(\frac{\mathrm{DIST}}{u^{(2)}(T_m) - v_n}\right)^2\right]. \tag{4.1d}$$

A simplified diagnostic diagram can be constructed by summing fixed identification numbers assigned to each of the four coefficients given in expressions (4.1). These identification numbers are added only when the corresponding coefficients given by

(4.1) indicate that the influence of neighboring dispersion curves is at least one-tenth of the amplitude along the ridge crest (i.e., influences must be $\leqq 20$ db down from the crest values). It is convenient to use 1, 2, 8 and 16 for the identification numbers corresponding to $B^{(1)}$, $C^{(1)}$, $B^{(2)}$, and $C^{(2)}$, respectively. The number 4 has been omitted, because interference is possible within a given mode when the group velocity curve has more than one branch. The figures representing the diagnostic pattern can be easily decomposed in terms of the four coefficients, above.

A synthetic seismogram with an aftershock is used in order to illustrate the principle of the diagnostic diagram. A synthetic vertical-component seismogram, representing the Rayleigh and the first shear modes (Figures 4 and 5) was altered by adding the same seismogram to itself after a delay of 30 sec, with an amplitude reduction of 0.5.

Two fragments of the multiple filter analysis of the resulting seismogram are shown on the left side of Figure 10. The velocity scale has been expanded twice in comparison with previous figures. Thick solid lines represent theoretical group velocities of the original signal, dashed lines indicate theoretical group velocities of the delayed signal. The solid contours correspond to 5 db variations in amplitude. Broken contours, drawn in regions of particular interest, show 1 db amplitude variations. Hatched areas are amplitude lows.

The corresponding diagnostic diagram is shown on the right side of Figure 10. The Rayleigh and the first shear modes are considered independently in the following discussion, since their separation in the velocity-period plane is sufficient to prevent any interference. Interactions between the original and delayed signals will serve to illustrate the method.

Consider the sums, N, calculated as above with a 20 db cut-off level, which appear at each element in the grid of the diagnostic diagram. The minus signs in the display only serve to delineate the theoretical group velocity curves. The absolute values of these sums can be decomposed to find the integral number of elements contributing, and the type of the interaction affecting any particular domain element as follows:

$$\begin{aligned}
&\text{No. of } \textit{frequency} \text{ interactions from delayed signal:}\\
&\quad n_{f2} = [N/16]\\
&\text{No. of } \textit{time} \text{ interactions from delayed signal:}\\
&\quad n_{t2} = [(N - n_{f2}\cdot 16)/8]\\
&\text{No. of } \textit{frequency} \text{ interactions from original signal:}\\
&\quad n_{f1} = [(N - n_{f2}\cdot 16 - n_{t2}\cdot 8)/2]\\
&\text{No. of } \textit{time} \text{ interactions from original signal:}\\
&\quad n_{t1} = 0 \text{ if } N \text{ is even, } = 1 \text{ if } N \text{ is odd,}
\end{aligned} \tag{4.2}$$

where square brackets imply the integral part of the result. For example, the element for $v = 2.64$ km/sec, $T = 12.5$ sec has the value of $N = 41$, which translates as $n_{f2} = 2$, $n_{t2} = 1$, $n_{f1} = 0$, $n_{t1} = 1$. Thus the amplitude calculated for this point of the grid will be affected by frequency domain interference from two branches of the delayed signal and by time domain interference from the original and the delayed signals.

Portions of the diagnostic diagram under the influence of the Rayleigh mode and the first shear mode corresponding to the original signal are marked with horizontal lines. Regions influenced by the delayed signal are marked with vertical lines. Note that the area of influence of the original signal is significantly larger. This results from the fact that the amplitudes of the original signal are twice as large as those for the delayed signal.

If the cut-off level of influence is chosen properly, the diagnostic diagram permits a

simple estimate of the period range in which group velocities can be correctly interpreted from the contour diagram. This, in terms of Figure 10, will be any portion of the group velocity curve which does not fall within the limits of influence of the other signal. The diagnostic diagram indicates, for example, that the contours should yield proper group velocity information within the interval from 3.5 sec to 8 sec for the Rayleigh mode of the original signal. It can be seen on the left side of Figure 10 that the contours closely follow the theoretical group-velocity curve within this range. Similar agreement can be found for the Rayleigh mode of the delayed signal, in a significantly smaller period range. Satisfactory results are also found at the short period

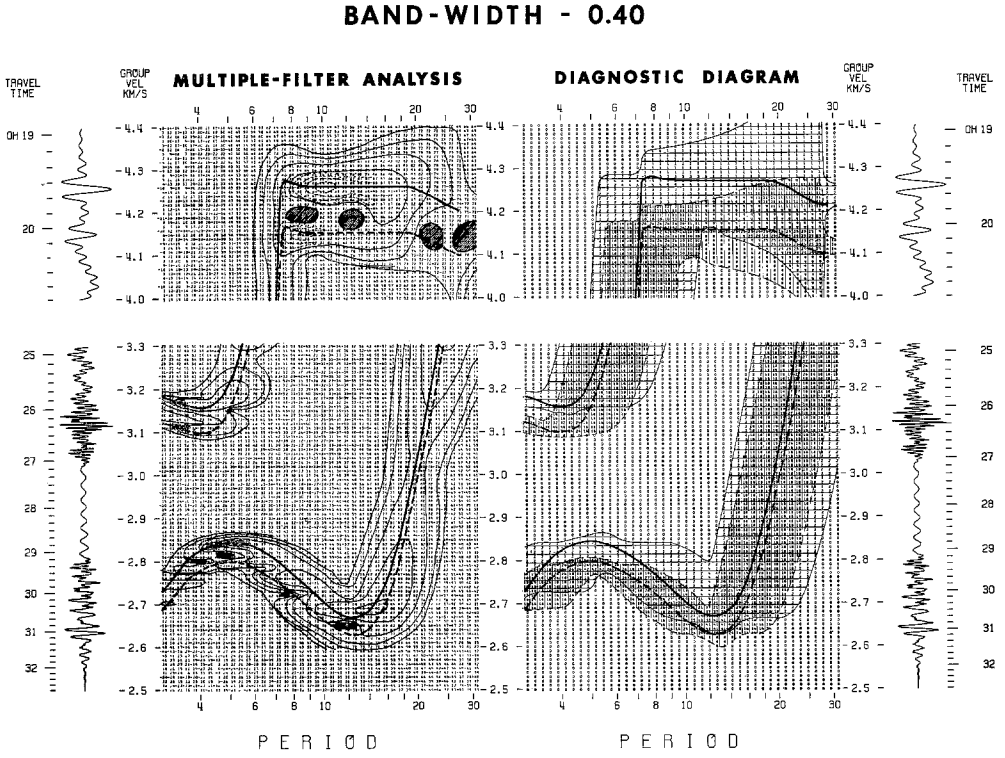

FIG. 11. Multiple filter analysis (left) and corresponding diagnostic diagram (right) calculated for the same seismogram as shown in Figure 10. Relative filter bandwidth = 0.40. Note improved resolution in regions where group velocity curve is flat. For further explanation see caption for Figure 10 and text, section 4.

ends of the first shear mode for both the original and the delayed signals. Only a short interval of the flat portion of the first shear mode of the original signal is not disturbed by the interfering signal.

Figure 11 represents the result of analysis of the same seismogram with a broader filter bandwidth. The relative bandwidth is here 0.40, while it was 0.25 in the previous case. The only improvement in the separation of these signals occurs in the flat portions of the first shear mode for both signals. This could have been expected, since the time resolution is improved by the increased bandwidth. The improvement in separation between signals is limited for the delayed signal, because the increase in time resolution is associated with a reduction in frequency resolution and a consequent broadening of the contours for the steep portions of the shear mode dispersion curve. The resolving power is less for the other regions of the display, compared to the results in Figure 10.

The comparison of Figures 10 and 11 illustrates the effect of the filter parameters on the analyzed result. It also shows that diagnostic diagrams provide a useful and reliable tool for selection of the filter bandwidth in order to analyze various portions of the dispersion curves. It is worthwhile to note that the expenditure of the computer time required for calculation of a diagnostic diagram is insignificant in comparison with the time needed for multiple filter analysis.

This type of diagram may prove to be useful in pretesting the results of the multiple filter analysis when the filter parameters are varied to suit the observed dispersion.

V. Conclusions

The multiple filter technique has been found to be a rapid, convenient method of analyzing multi-mode dispersed signals. Its time and frequency resolution can be checked with the aid of a simple diagnostic diagram. These techniques should have great utility in studies of recorded transient signals.

Acknowledgments

The authors are grateful to Dr. Flavian Abramovici for discussions and suggestions regarding the properties of filter functions. They wish to thank Dr. Anton L. Hales for his encouragement and for many helpful remarks. The authors are also grateful to Dr. John W. Graham for critically reading the manuscript.

This study was supported by the National Science Foundation under grants GA-830 and GA-1404, by the National Aeronautics and Space Administration, under NsG-269-62 with the Southwest Center for Advanced Studies and by supplemental research funds of the latter institution. The development of the technique reported in this paper was also supported by the Office of Naval Research under contract N00014-67-0310-0001.

References

Alexander, S. S. (1963). *Surface Wave Propagation in the Western United States* (Ph.D. Thesis), California Institute of Technology, 241 pp.

Archambeau, C. B., E. A. Flinn, and D. G. Lambert (1966). Detection, analysis, and interpretation of teleseismic signals, 1, compressional phases from the Salmon event, *J. Geophys. Res.*, **71,** 3483–3501.

Bloch, S., and A. L. Hales (1968). New techniques for the determination of surface wave phase velocities, *Bull. Seism. Soc. Am.*, **58,** 1021–1036.

Cooley, J. W., and J. W. Tukey (1965). An algorithm for the machine calculation of complex Fourier series, *Mathamatics of Computation*, **19,** 297–301.

Goodman, N. R. (1960). Measuring amplitude and phase, *J. Franklin Inst.*, **260,** 437–450.

Landisman, M., A. Dziewonski, Y. Satô, and R. Massé (1968). Preliminary report on recent improvements in the analysis of surface waves, *Proc. of the Fourth Int. Symp. on Geophysical Theory and Computers, Nuovo Cimento (Supplement)*, **6,** No. 1, 126–131.

Landisman, M., A. Dziewonski, and Y. Satô (1969). Recent improvements in the analysis of surface wave observations, *Geophys. J.R.A.S.*, (in press).

Ormsby, J. F. (1961). Design of numerical filters with application to missile data processing, *J. Assoc. Computing Mach.*, **8,** 440–466.

Papoulis, A. (1962). *The Fourier Integral and Its Applications*, McGraw-Hill, New York, 318 pp.

Slepian, D., H. O. Pollack, and H. J. Landau (1961). Prolate spheroidal wave functions, Fourier analysis and uncertainty, *Bell Telephone System Tech. Publ., Monograph 3746.*

Southwest Center for Advanced Studies
P. O. Box 30365
Dallas, Texas 75230
Contribution No. 86

Manuscript received July 25, 1968.